RSC Advances

PAPER

View Article Online
View Journal | View Issue

Cite this: *RSC Adv.*, 2024, **14**, 18432

Efficient removal of methyl orange and ciprofloxacin by reusable Eu–TiO_2/PVDF membranes with adsorption and photocatalysis methods†

Jiao Wang, * Hemu Pi, Panchao Zhao and Na Zhou

The presence of methyl orange (MO) and ciprofloxacin (CIP) in wastewater poses a serious threat to the environment and human health. Titanium dioxide nanoparticles (TiO_2 NPs) are widely studied as photocatalysts for wastewater treatment. However, TiO_2 NPs have the drawbacks of high energy required for activation, fast electron–hole pair recombination and difficulty in recovering from water. To overcome these problems, europium decorated titanium dioxide/poly(vinylidene fluoride) (Eu–TiO_2/PVDF) membranes were successful prepared in this work by combining the modified sol–gel method and the immersion phase inversion method. The Eu–TiO_2/PVDF membranes obtained with the increase of Eu–TiO_2 NPs content during the preparation process were named M1, M2 and M3, respectively. The pure PVDF membrane without the addition of Eu–TiO_2 NPs was named M0, which was prepared by the immersion phase inversion method and served as a reference. The prepared Eu–TiO_2/PVDF membranes could not only adsorb MO, but also degrade CIP under visible-light irradiation. Moreover, the Eu–TiO_2/PVDF membranes exhibited adsorption–photocatalytic activity towards a mixture of MO and CIP under visible-light irradiation. Last but not the least, the Eu–TiO_2/PVDF membranes exhibited excellent recyclability and reusability, opening the avenue for a possible use of these membranes in sewage-treatment plants.

Received 22nd April 2024
Accepted 3rd June 2024

DOI: 10.1039/d4ra02962c

rsc.li/rsc-advances

1. Introduction

Dyes and antibiotics are detected frequently in wastewater, due to their widespread application.[1–3] Methyl orange (MO), as a typical azo dye, has been used to dye textiles.[4,5] It contains a nitrogen to nitrogen double bond (–N=N–), which is difficult to be degraded.[6,7] Due to its toxicity and water solubility, the presence of MO in water is very harmful to human health and the environment.[5,6] Ciprofloxacin (CIP), as a common antibiotic, is heavily used as the medicine in human activities.[8,9] Its residue can cause eco-toxicological effects and enhance the resistance of bacteria in water.[8–10] Therefore, the removal of MO and CIP from wastewater is an urgent problem to be solved.

However, traditional wastewater treatment methods, including flocculation, reverse osmosis, precipitation and ion exchange, have some limitations such as expensive equipment, secondary pollution, slow treatment rate and complex operation.[11–13] Photocatalysis, as an important method in advanced oxidation progresses, has become a research hotspot in wastewater treatment due to its green energy-saving, easy operation, safety, low cost and no secondary pollution.[14–16]

As a typical photocatalyst, titanium dioxide (TiO_2) has been used in photocatalysis because of its non-toxicity, low cost and chemical inertness.[17,18] However, TiO_2 has a large bandgap, which is needed for photocatalytic degradation of pollutants in water under ultraviolet (UV) irradiation.[19] UV radiation accounts for only 5% of the energy in solar radiation, while visible light accounts for 43%.[20] Therefore, improving the visible-light photocatalytic activity of TiO_2 can better utilize solar light, thereby saving energy. In this work, TiO_2 was decorated with the rare earth metal europium (Eu) to enhance its photocatalytic activity under visible-light irradiation. The specific benefits of Eu modified TiO_2 are as follows: (1) the decoration of Eu can narrow the bandgap of TiO_2 to achieve its absorption of visible light; (2) the f orbitals of Eu can interact with the functional groups in different pollutants to form complexes, thereby improving its adsorption capacity for pollutants.[21]

However, europium–titanium dioxide nanoparticles (Eu–TiO_2 NPs) are easily washed away and cannot be well recovered in wastewater treatment due to their small particle size. In order to solve this problem, poly(vinylidene fluoride) (PVDF) membranes[22] with good film-forming properties, high mechanical strength and stable chemical properties were

Northwest Institute for Non-ferrous Metal Research, Xi'an, 710016, Shaanxi, P. R. China. E-mail: wjiao0311@163.com

† Electronic supplementary information (ESI) available. See DOI: https://doi.org/10.1039/d4ra02962c

prepared for the support of Eu–TiO_2 NPs and serve as excellent adsorbents in water treatment. In this work, Eu–TiO_2/PVDF membranes with different Eu–TiO_2 NPs contents were prepared *via* the modified sol–gel method and the immersion phase inversion method. With the increase of Eu–TiO_2 NPs content, the obtained Eu–TiO_2/PVDF membranes were named M1, M2 and M3, respectively. The pure PVDF membrane without the addition of Eu–TiO_2 NPs was named M0, which was prepared by the immersion phase inversion method and served as a reference. The obtained Eu–TiO_2/PVDF membranes could not only adsorb MO, but also degrade CIP under visible-light irradiation. In order to study the adsorption or photocatalytic activity and mechanism of Eu–TiO_2/PVDF membranes, the adsorption kinetics, adsorption isotherms and photocatalytic kinetics experiments were conducted and analysed. Moreover, the Eu–TiO_2/PVDF membranes exhibited adsorption–photocatalytic activity towards a mixture of MO and CIP under visible-light irradiation. Finally, the Eu–TiO_2/PVDF membranes exhibited good regeneration and reusability after adsorption–photocatalytic degradation of a mixture of MO and CIP.

2. Experimental section

2.1 Materials

Tetrabutyl titanate (TBOT, 98%), ethanol (CH_3CH_2OH, 99.5%), acetic acid (CH_3COOH, 99.8%), dimethylacetamide (DMAc, 99%), methyl orange (MO, 85%) and hydrochloric acid (HCl, 37%) were purchased from Sinopharm Chemical Reagent Co., Ltd (Shanghai, China). Polyvinyl pyrrolidone K30 (PVP) was purchased from Tokyo Chemical Industry Co., Ltd (Tokyo, Japan). Europium nitrate hexahydrate ($Eu(NO_3)_3 \cdot 6H_2O$, 99.9%), poly(vinylidene fluoride) (PVDF) and ciprofloxacin (CIP, 98%) were purchased from Aladdin Reagents Co., Ltd (Shanghai, China).

2.2 Preparation of Eu–TiO_2 NPs

The modified sol–gel method was used to prepare Eu–TiO_2 NPs.[23] Firstly, 10 mL of TBOT and 30 mL of ethanol were mixed together under stirring for 10 min to get a transparent yellow sol, which is labelled as solution A. Secondly, 0.065 g of $Eu(NO_3)_3 \cdot 6H_2O$ were dissolved into 10 mL of ethanol. After complete dissolution, 10 mL of ultrapure water and 5 mL of acetic acid were added into the former solution to obtain solution B. Solution A was added dropwise to solution B under stirring to form a mixture. After a while, the mixture was put under room temperature to get the gel. The gel was dried at 80 °C for 7 h and then calcined at 500 °C for 2 h to obtain Eu–TiO_2 NPs.

2.3 Preparation of the membranes

Eu–TiO_2/PVDF membranes were prepared *via* the immersion phase inversion method.[24,25] Firstly, the predetermined quantities of Eu–TiO_2 NPs were dispersed in 12 mL of DMAc solvent under stirring. Subsequently, 2 g of PVDF and 0.8 g of PVP were added into the former suspension with sonication to obtain the homogenous solution. After 1 h sonication, the solution was heated for 8 h at 70 °C under stirring to obtain the casting solution. The casting solution was casted on the cleaned polyethylene terephthalate (PET) film and immersed into ultrapure water. After a while, the membrane was naturally separated from the PET substrate. The obtained Eu–TiO_2/PVDF membranes were immersed in ultrapure water for 24 h and then dried at room temperature. With the increase of Eu–TiO_2 NPs content, the Eu–TiO_2/PVDF membranes were named M1, M2 and M3, respectively. Pure PVDF membrane (M0) without the addition of Eu–TiO_2 NPs was prepared by the same immersion phase inversion method. The compositions of M0, M1, M2 and M3 are shown in Table 1.

Table 1 The compositions of M0, M1, M2 and M3

Membrane compositions	M0	M1	M2	M3
PVDF (g)	2	2	2	2
PVP (g)	0.8	0.8	0.8	0.8
DMAc (mL)	12	12	12	12
Eu–TiO_2 (g)	0	0.02	0.2	0.4

2.4 Characterisation of the membranes

Scanning electron microscopy (SEM) SU5000 (Hitachi, Japan) was used to analyse the structure and morphology of the membranes. All membranes were treated with platinum sputter coating prior to SEM observation. The chemical compositions of the membranes were examined by Fourier Transform Infrared (FTIR) spectroscopy (Nicolet IS10, Thermo Nicolet Corporation, USA). IR spectra were acquired in transmission mode and the wavenumber range was from 4000 to 500 cm^{-1}. The crystalline phase of all samples was investigated by a Bruker D8-Advance X-ray diffraction (XRD) system (Germany). The wettability of water droplets on the membranes' surface was characterized by using an optical contact angle measurements instruments (Dataphysics OCA50, Germany). Thermogravimetric analyses (TGA) were performed using a Netzsch STA 409 F3 thermal analyser (Germany). The membranes were heated from 25 to 600 °C (10 °C min^{-1}) and under argon atmosphere (50 mL min^{-1}). The Brunauer–Emmett–Teller (BET) surface area of the membranes was computed from the N_2 adsorption–desorption isotherms by using the TriStar II Plus 3.03 (Micromeritics, USA).

2.5 Adsorption experiments

All adsorption experiments on the membranes were performed under dark conditions and at room temperature with a constant stirring rate. MO absorbance changes were monitored by using an ultraviolet-visible (UV-Vis) spectrophotometer (UV 3600, Shimadzu, Japan). The maximum absorbance of the MO aqueous solution was at 463 nm. For the adsorption kinetic experiments, 20 cm^2 of the membranes were added into 50 mL of the MO aqueous solution (3 mg L^{-1}) under stirring and dark conditions. During the adsorption, samples were taken at different adsorption times of 10 min, 20 min, 30 min, 60 min,

90 min, 120 min, 150 min and 180 min. For the adsorption mechanism experiments, 20 cm^2 of the membranes were added to each of the MO aqueous solution (50 mL) with different initial concentrations under dark conditions and stirring. The initial concentrations of the MO aqueous solution were 1, 3, 5, 20, 30, 60 and 90 mg L^{-1}, respectively. Samples were taken after 180 min adsorption.

The equilibrium adsorption capacity q_e (mg g^{-1}) was calculated by using eqn (1):[26–28]

$$q_e = \frac{(C_0 - C_e)V}{m} \quad (1)$$

where C_0 (mg L^{-1}) and C_e (mg L^{-1}) were the initial and equilibrium concentrations of the pollutant, V (L) was the volume of the pollutant solution, and m (g) was the mass of the membranes.

The pseudo-first-order (eqn (2)) and pseudo-second-order (eqn (3)) models were used to evaluate the adsorption kinetics of the membranes towards the pollutant.[29]

$$\mathrm{Ln}(q_e - q_t) = \ln q_e - k_1 t \quad (2)$$

$$\frac{t}{q_t} = \frac{1}{k_2 q_e^2} + \frac{t}{q_e} \quad (3)$$

where q_t (mg g^{-1}) was the adsorption capacity at time t (min), k_1 (min^{-1}) and k_2 (g (mg^{-1} min^{-1})) were the pseudo-first-order and pseudo-second-order rate constants, respectively.

Langmuir (eqn (4)) and Freundlich (eqn (5)) adsorption models were used to investigate the adsorption mechanism of the membranes towards the pollutant.[30,31]

$$\frac{C_e}{q_e} = \frac{1}{K_L q_m} + \frac{C_e}{q_m} \quad (4)$$

$$\mathrm{Log}\ q_e = \log K_F + \frac{1}{n}\log C_e \quad (5)$$

where C_e (mg L^{-1}) was the equilibrium concentration of the pollutant, q_e (mg g^{-1}) was the equilibrium adsorption capacity, q_m (mg g^{-1}) was the maximum adsorption capacity, K_L and K_F were the Langmuir and Freundlich adsorption equilibrium constants, and n was a constant related to adsorption intensity.

2.6 Photocatalytic experiments

The photocatalytic activity of the membranes was evaluated by the degradation of CIP under visible-light irradiation. A CEL-HXF300-T3 xenon lamp (China Education Au-light Co., Ltd, Beijing, China) with a UVIRCUT 420 filter for obtaining light at wavelength ranging from 420 to 780 nm was used as a visible-light source. 20 cm^2 of the membranes were added into 50 mL of the CIP aqueous solution (3 mg L^{-1}) under stirring. The mixture was kept in the dark for 30 min to establish the adsorption–desorption equilibrium. Subsequently, the mixture was placed under visible-light irradiation and samples were withdrawn at times 0 min (before irradiation) and after 10 min, 20 min, 30 min, 60 min, 90 min, 120 min, 150 min, 180 min, 210 min of visible-light irradiation. The absorbance changes for CIP were monitored by UV-Vis spectroscopy and the maximum absorbance of the CIP aqueous solution was at 277 nm. The obtained photocatalytic degradation curve was fitted by using a pseudo-first-order kinetic model as in eqn (6):[32]

$$-\mathrm{Ln}\frac{C_t}{C_0} = kt \quad (6)$$

where C_t (mg L^{-1}) was the pollutant concentration at time t (min), C_0 (mg L^{-1}) was the pollutant concentration at time zero, and k (min^{-1}) was the degradation rate constant.

2.7 Adsorption–photocatalysis experiments

A mixture of MO and CIP was used as a mixed pollutants model to evaluate the adsorption–photocatalytic activity of the Eu–TiO_2/PVDF membranes. Firstly, a mixed solution of MO and CIP ($C_{MO} = C_{CIP} = 1$ mg L^{-1}) was prepared. 20 cm^2 of the Eu–TiO_2/PVDF membrane (M2) were added into 50 mL of the aforementioned mixed solution under stirring and dark conditions for 180 min to reach the adsorption–desorption equilibrium. During the adsorption process, samples were withdrawn at 30 min, 60 min, 90 min, 120 min, 150 min and 180 min. Subsequently, the former mixture was placed under visible-light irradiation with stirring for 180 min. During this process, samples were withdrawn at 0 min (equivalent to 180 min of the former adsorption process), 30 min, 60 min, 90 min, 120 min, 150 min and 180 min after visible-light irradiation. The absorbance changes of all samples were monitored by UV-Vis spectroscopy.

Besides, a similar procedure was followed for the recycling adsorption–photocatalysis experiments: after each adsorption–photocatalysis experiment, M2 was washed by 0.1 M HCl and ultrapure water, dried, and reused for the subsequent adsorption–photocatalysis experiment of a fresh MO and CIP solution.

3. Results and discussion

3.1 Preparation and characterisation of the membranes

The preparation pathway for the Eu–TiO_2/PVDF membranes (M1, M2 and M3) is illustrated in Scheme 1. The experiment details are reported in the Experimental section. The Eu–TiO_2/PVDF membranes (M1, M2 and M3) were prepared by the combination of the modified sol–gel method and the immersion phase inversion method. Pure PVDF membrane (M0) without the addition of Eu–TiO_2 NPs was prepared by the immersion phase inversion method. The morphology and structure of all membranes were characterised by SEM measurements.

Fig. 1(a) shows the SEM image of the pure PVDF membrane (M0), which has a smooth surface. Most of the pores on M0 are at the micrometer level, with only a small portion at the nanometer level. Fig. 1(b)–(d) show the SEM images of Eu–TiO_2/PVDF membranes (M1, M2 and M3) with different contents of Eu–TiO_2 NPs, respectively. The porous size of M1, M2 and M3 is also from nano to micro scale. When the Eu–TiO_2 NPs content of the membranes increases, the pores on the membranes become smaller, and the number of pores on the membranes also decrease. Among them, M3 has the smallest number of pores.

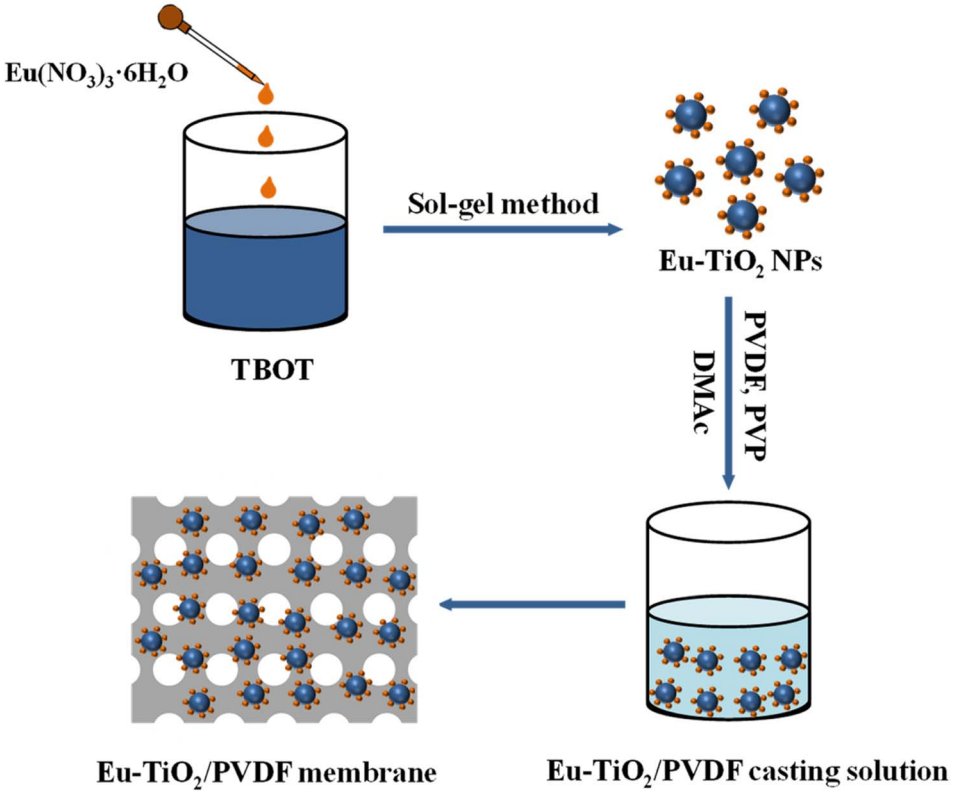

Scheme 1 Steps for preparing the Eu–TiO_2/PVDF membrane.

The possible reason is that the excessive mixed Eu–TiO_2 NPs aggregation, which blocks the pores of the membrane and reduces its pore size.[33,34]

EDS analyses of Eu–TiO_2/PVDF membranes (M1, M2 and M3) were performed and the results were collected in Fig. S1, S2 and Table S1.† According to EDS analyses, the main structural elements of M1, M2 and M3 are carbon (C), oxygen (O) and fluorine (F), as expected. Platinum (Pt) was detected on all membranes, because all membranes were sputtered with Pt before SEM testing to ensure good conductivity. The presence of titanium (Ti) in M2 and M3 confirmed that the presence of TiO_2. However, there was no Ti in M1, which might be the lower content of TiO_2 of M1. Furthermore, the element composition determined by EDS showed that the weight percentage of C, O, F, Pt and Ti. In Table S1,† C, O and F accounted for the main percentage in M1, M2 and M3, while Ti had a relatively low percentage. The weight percentage of Ti in M1, M2 and M3 was 0, 0.03% and 1.83%, respectively.

IR spectra of M0, M1, M2 and M3 are shown in Fig. 2(a). All membranes exhibited distinct characteristic peaks of PVDF, which included $-CH_2$ bending (1402 cm^{-1}), $-CF_2$ stretching (1174 cm^{-1}) and amorphous phase absorption (876 and 839 cm^{-1}).[28,35,36] The peak with less intensity at 1664 cm^{-1} was due to C=O stretching vibration of PVP.[37] The spectra suggested that no changes occurred after the mixture of PVDF with Eu–TiO_2 NPs and no residual solvent left on the membranes.

XRD patterns of the pure PVDF membrane (M0) and Eu–TiO_2/PVDF membranes (M1, M2 and M3) are displayed in Fig. 2(b). M0 showed the diffraction peaks at 18.47, 20.24 and 26.88, corresponding to PVDF, with (020), (110) and (021) diffraction planes.[38] Obviously, the characteristic peaks of PVDF appeared in M1, M2 and M3. Furthermore, for both M2 and M3, in addition to the characteristic peaks of PVDF, new peaks were observed at 25.45, 38.88 and 48.83, corresponding to TiO_2, with (101), (004) and (200) planes. These results confirmed the successful incorporation of TiO_2 NPs into the membranes. For M1, the characteristic peaks of TiO_2 were not obvious, because the mass of Eu–TiO_2 NPs was much lower than that of PVDF. These results are consistent with the characterization results of EDS mapping (Fig. S1, S2 and Table S1†).

Thermal stability is an important criterion for Eu–TiO_2/PVDF membranes before applying these membranes to different applications. Fig. 3 illustrates the TGA curves of the pure PVDF membrane (M0) and Eu–TiO_2/PVDF membranes (M1, M2 and M3). When the heat treatment temperature was in the range of 300–500 °C, the weight loss of all membranes was notable. The degradation temperature was shifted from 304 °C (for M0) to 373 °C (for M3), which indicated that the thermal stability of membranes increased with the enhancement of Eu–TiO_2 NPs amount.[22,39] In addition, the results showed that the residual mass of M0, M1, M2 and M3 was 40%, 42%, 44% and 61% at 600 °C, respectively. The pure PVDF membrane showed higher weight loss than Eu–TiO_2/PVDF membranes, which was due to the enhancement of Eu–TiO_2 NPs amount and the good interfacial interactions between PVDF and Eu–TiO_2 NPs.[22,39]

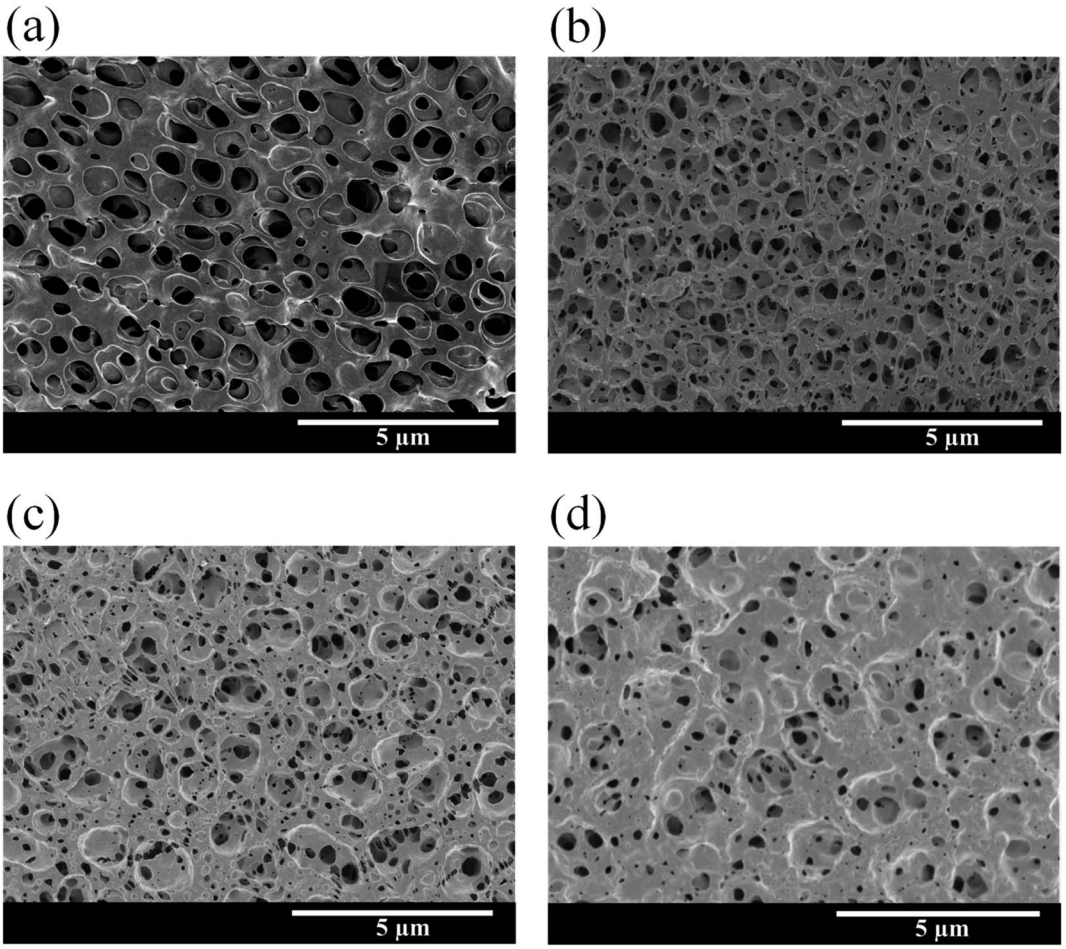

Fig. 1 SEM images of (a) M0, (b) M1, (c) M2 and (d) M3.

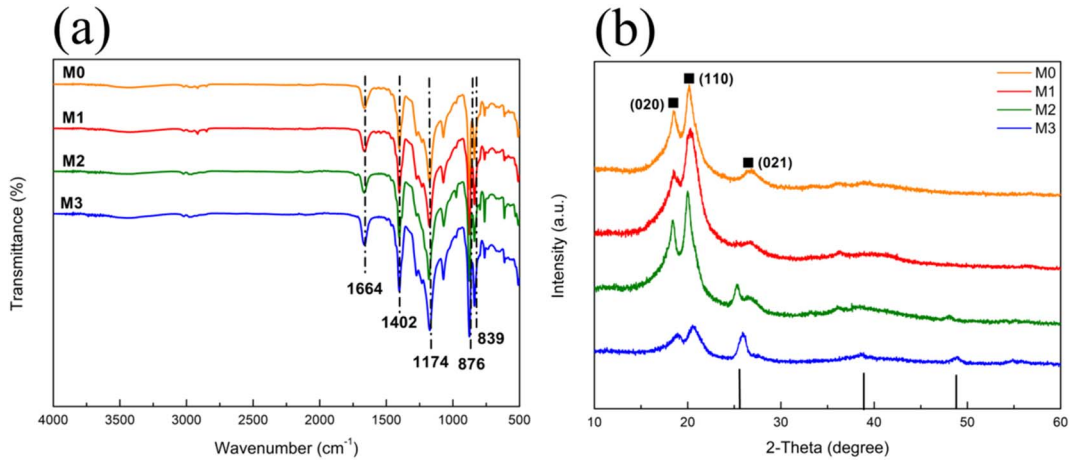

Fig. 2 (a) IR spectra and (b) XRD patterns of M0 (orange line), M1 (red line), M2 (green line) and M3 (blue line).

The water contact angle for exploring the hydrophilicity of the membranes is shown in Table 2. The contact angle of the pure PVDF membrane (M0) was about 114 ± 6°, which suggested that the surface of the pure PVDF membrane (M0) was hydrophobic.[40] The contact angle was about 108 ± 7° for M1, 92 ± 7° for M2 and 56 ± 4° for M3, indicating that the contact angle of the membrane decreased with the increase of Eu–TiO_2 NPs content in the membrane. The possible reason was that the presence of Eu–TiO_2 NPs with a large number of hydrophilic groups (Ti–OH) made the membranes hydrophilicity thereby

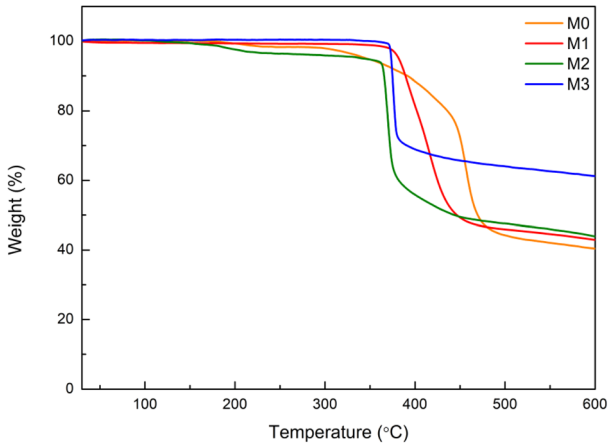

Fig. 3 TGA measurements for M0 (orange line), M1 (red line), M2 (green line) and M3 (blue line).

Table 2 Contact angles of the membranes with different content of Eu–TiO_2 NPs (M0, M1, M2 and M3)

Membranes	Content of Eu–TiO_2 (g)	Average contact angle (°)
M0	0	114 ± 6
M1	0.02	108 ± 7
M2	0.2	92 ± 7
M3	0.4	56 ± 4

reducing the value of water contact angle.[37] In a word, a decrease in contact angle lead to an increase in the hydrophilicity of the membrane, which is beneficial for its future application in water treatment.

The N_2 adsorption–desorption isotherm in Fig. 4 was carried out to determine the specific surface area of M0, M1, M2 and M3. As shown in Table 3, the BET surface area of M0, M1, M2 and M3 was 16.5258, 20.5867, 20.4360 and 26.0562 $m^2\ g^{-1}$, respectively. Compared with the BET surface area of the pure PVDF membrane (M0), the BET surface area of Eu–TiO_2/PVDF membranes (M1, M2 and M3) increased, which was attributed to the introduction of Eu–TiO_2 NPs. After introducing Eu–TiO_2 NPs, the proportion of the smaller pore sizes increased quickly, while the large void structures decreased or even disappeared.[41]

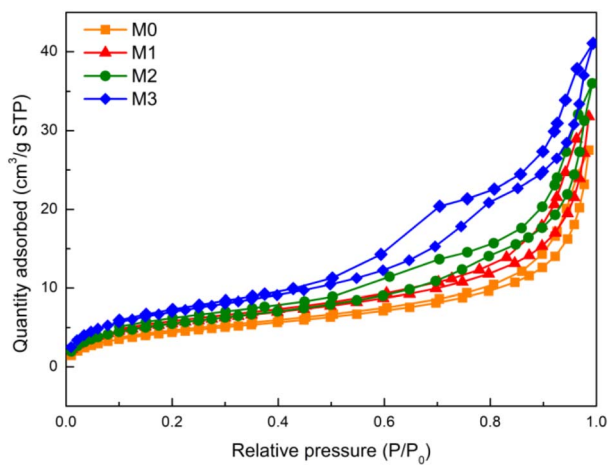

Fig. 4 Nitrogen adsorption–desorption isotherm of M0 (orange line), M1 (red line), M2 (green line) and M3 (blue line).

Table 3 The specific surface area of M0, M1, M2 and M3 by BET test

Membranes	M0	M1	M2	M3
Specific surface area ($m^2\ g^{-1}$)	16.5258	20.5867	20.4360	26.0562

3.2 Adsorption capacity of the membranes towards MO

MO was selected as a target pollutant to evaluate the adsorption capacity of M0, M1, M2 and M3, respectively. The chemical structure of MO is shown in Fig. S3(a).† Fig. 5 shows the adsorption kinetics curves of MO on M0, M1, M2 and M3. The adsorption percentage of MO was 75% by M0, 36% by M1, 39% by M2 and 27% by M3. The data indicated that the adsorption capacity of the pure PVDF membrane (M0) was better than Eu–TiO_2/PVDF membranes (M1, M2 and M3). The possible reason is that the excessive mixed Eu–TiO_2 NPs aggregation, which blocks the pores of the membrane and reduces its pore size and pore numbers.[34] As a result, the active sites of the membranes reduced, which prevented the adsorption of MO to the membranes.

The fitting of pseudo-first-order (eqn (2)) and pseudo-second-order (eqn (3)) model is shown in Fig. S4 and S5,† respectively, and the kinetic constants are listed in Table 4. The results indicate that the kinetic data of MO by M0, M1, M2 and M3 are better fitted with the pseudo-first-order model than with the pseudo-second-order. Because for M0, M1 and M3, the correlation coefficient value of the pseudo-first-order model (R^2 = 0.9781 for M0, 0.9638 for M1, 0.9611 for M3) is higher than the one of the pseudo-second-order model (R^2 = 0.9042 for M0, 0.9127 for M1, 0.9401 for M3). And for M2, the theoretical

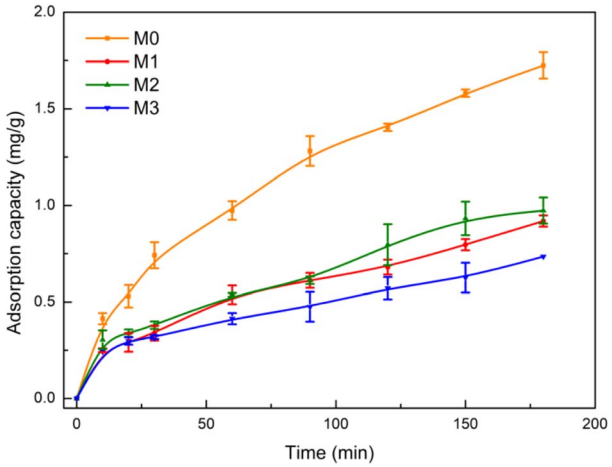

Fig. 5 Adsorption kinetic curves of MO by M0 (orange line), M1 (red line), M2 (green line) and M3 (blue line) under dark conditions (initial concentration of MO: 3 mg L^{-1}).

Table 4 Model parameters of adsorption kinetics for MO adsorption on M0, M1, M2 and M3

		Pseudo-first-order model			Pseudo-second-order model		
Membranes	$q_{e,exp}$ (mg g^{-1})	q_e (mg g^{-1})	k_1 (min^{-1})	R^2	q_e (mg g^{-1})	k_2 (g (mg^{-1} min^{-1}))	R^2
M0	1.73	1.66	0.01527	0.9781	1.79	0.01695	0.9042
M1	0.92	1.20	0.01203	0.9638	0.86	0.04035	0.9127
M2	1.02	1.02	0.01757	0.8551	0.98	0.03292	0.8664
M3	0.73	0.62	0.01181	0.9611	0.65	0.07445	0.9401

equilibrium adsorption capacity of the pseudo-first-order (1.02 mg g^{-1}) is the same with the actual equilibrium adsorption capacity ($q_{e,exp}$ = 1.02 mg g^{-1}). It is usually observed that when adsorption diffusion occurs through the interface, the dynamics follow this pseudo-first-order equation.[27] The adsorption kinetics of M0, M1, M2 and M3 towards MO are more fit the pseudo-first-order model, suggesting that the adsorption rate decreased linearly with the increase of adsorption capacity.[27,29]

The experimental adsorption isotherm for MO adsorption on M0, M1, M2 and M3 (Fig. 6) indicates that the maximum adsorption capacity of the membranes towards MO reached 3.5, 4.8, 2.2 and 4.7 mg g^{-1}, respectively, after 180 min of adsorption. Langmuir and Freundlich adsorption isotherms obtained using eqn (4) and (5) are presented in Fig. S6 and S7,† and the parameters are listed in Table 5. The Langmuir adsorption model states that the adsorption of the adsorbate is limited to a single layer and the adsorbent sites are homogeneous.[26,42] It means that there is no interaction between the adsorbents, and each adsorbent occupies only one adsorption site. The Freundlich adsorption model implies multilayer adsorption, which results in different adsorption energies, because the adsorption sites on the surface of the adsorbent are heterogeneous.[26] Fig. S6, S7† and Table 5 indicate that the data of M0, M1 and M2 are better fitted with the Langmuir adsorption model than with the Freundlich one, and the data of M3 are better fitted with the

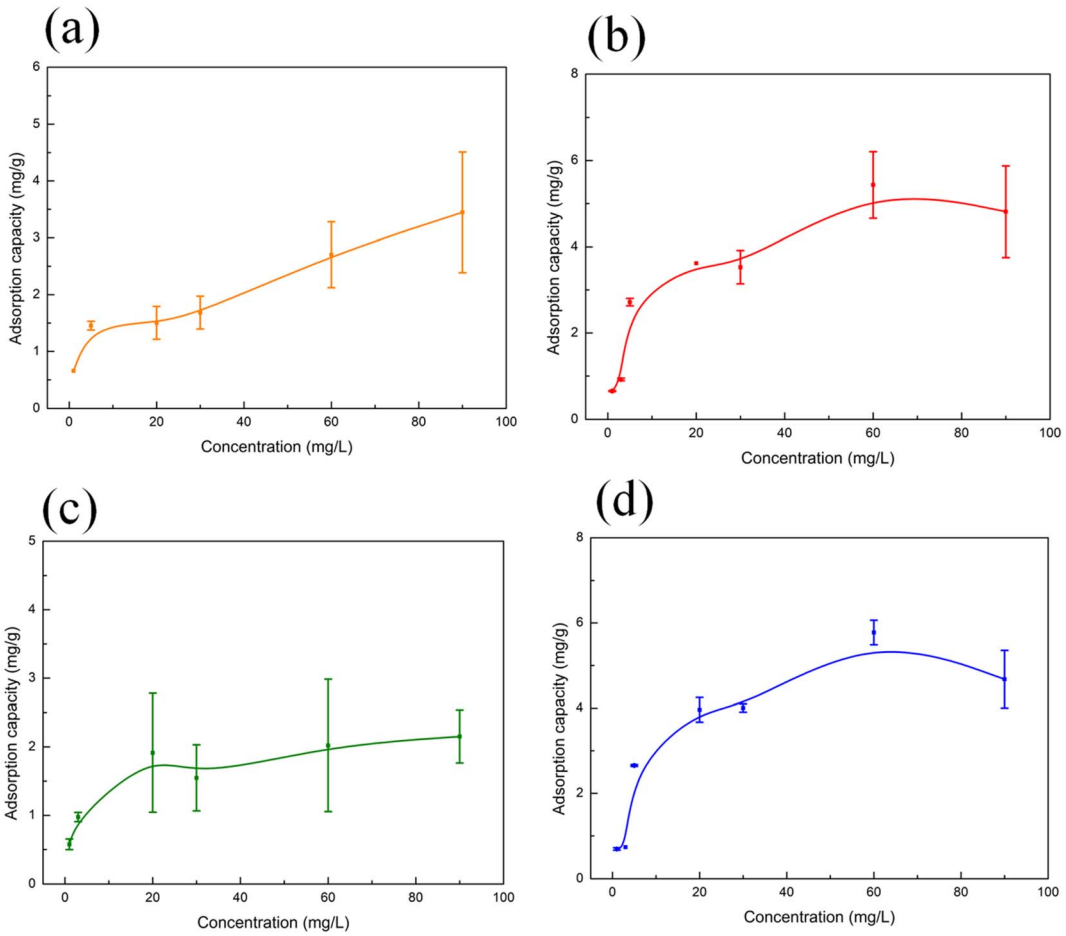

Fig. 6 Adsorption isotherm curves of MO by (a) M0, (b) M1, (c) M2 and (d) M3 under dark conditions.

Table 5 Model parameters of the Langmuir and Freundlich models for MO adsorption on M0, M1, M2 and M3

	Langmuir constants			Freundlich constants		
Membranes	K_L (L mg^{-1})	q_m (mg g^{-1})	R^2	K_F (mg g^{-1})	$1/n$	R^2
M0	0.1101	3.23	0.8736	1.23	0.1699	0.6653
M1	0.2354	5.05	0.9717	1.43	0.3011	0.7740
M2	0.3092	2.05	0.9738	1.08	0.1592	0.4072
M3	0.2564	5.12	0.9590	1.29	0.4106	0.9808

Freundlich adsorption model than with the Langmuir one. The evidence is that for M0, M1 and M2, the correlation coefficient value of the Langmuir adsorption model ($R^2 = 0.8736$ for M0, 0.9717 for M1, 0.9738 for M2) is higher than the one of the Freundlich adsorption model ($R^2 = 0.6653$ for M0, 0.7740 for M1, 0.4072 for M2). However, for M3, the correlation coefficient value of the Freundlich adsorption model ($R^2 = 0.9808$) is higher than the one of Langmuir adsorption model ($R^2 = 0.9590$). Therefore, the adsorption sites on the surface of M0, M1 and M2 are uniform and the rate determining step in the adsorption process is the interaction between MO and the adsorption sites of the membranes (M0, M1 and M2). It can be presumed that the adsorption of MO on M0, M1 and M2 mainly occurs through MO to the porous structure on the membranes. As for M3, the adsorption sites on its surface are heterogeneous with the different adsorption energies, that is, the active site of the adsorption is more than one. The possible adsorption mechanism of M3 is that MO adsorbed through porous structure and the Eu–TiO_2 NPs effect on M3.

3.3 Photocatalytic activity of the membranes towards CIP under visible-light irradiation

CIP was selected to evaluate the photocatalytic activity of the membranes under visible-light irradiation. The chemical structure of CIP is shown in Fig. S3(b).† The concentration of CIP is barely changed under visible-light irradiation in the absence of the photocatalyst (Fig. S8(a)†). The photodegradation of CIP was studied by acquiring the absorption spectra of the CIP solution at different times of visible-light irradiation in the presence of M0, M1, M2 and M3, as shown in Fig. S9.†

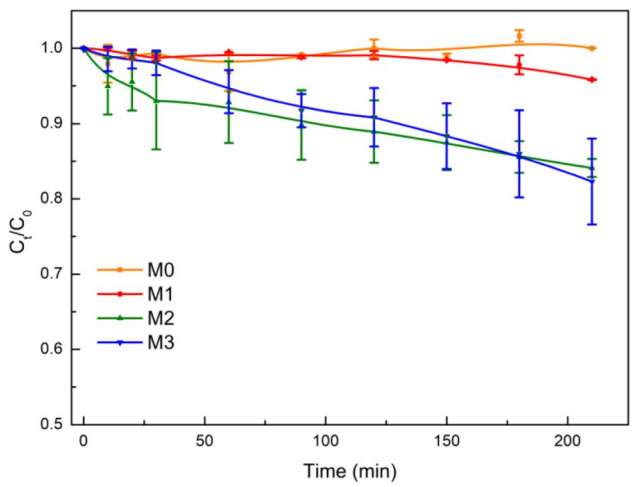

Fig. 7 Time-dependent variation of the concentration of CIP solution exposure to visible light in the presence of M0 (orange line), M1 (red line), M2 (green line) and M3 (blue line) (initial concentration of CIP: 3 mg L^{-1}).

Table 6 Photocatalytic degradation efficiency and degradation rate constants for CIP on M0, M1, M2 and M3

Membranes	Degradation efficiency (%)	k (min^{-1})
M0	0	0
M1	4	3.2×10^{-6}
M2	16	6.9×10^{-4}
M3	21	8.8×10^{-4}

In Fig. 7, the variation of CIP concentration over time shows that after 210 min of visible-light exposure, the concentration of CIP decreased by 0, 4%, 16% and 21% in the presence of M0, M1, M2 and M3, respectively. The results show that there was no degradation of CIP in the presence of M0 under visible-light irradiation, because of the absence of Eu–TiO_2 NPs. Besides, when using photocatalysts from M1 to M3, the photocatalytic degradation efficiency of CIP increased. The possible reason is that the content of Eu–TiO_2 NPs increased from M1 to M3. Therefore, Eu–TiO_2 NPs played a photocatalytic role in the membranes.

The pseudo-first-order kinetic model (eqn (6)) is used to analyse the degradation kinetics of CIP by the membranes. Fig. S10† and Table 6 show that the degradation rate constant of CIP in the presence of M1, M2 and M3 was 3.2×10^{-6}, 6.9×10^{-4} and 8.8×10^{-4} min^{-1}, respectively. The degradation rate constant for M3, in the case of CIP, was about 1.3 times higher than that for M2 and was about 275 times higher than that for M1. It could be ascribe that the content of Eu–TiO_2 NPs in M3 was 2 times higher than that of M2 and was 20 times higher than that of M1. The results indicated that within a certain range, as the Eu–TiO_2 NPs content of the membranes increased, the photocatalytic degradation efficiency of the Eu–TiO_2/PVDF membranes towards CIP increased.

3.4 Adsorption–photocatalytic activity of the membrane towards a mixture of MO and CIP

The adsorption–photocatalytic activity of the Eu–TiO_2/PVDF membrane towards a mixture of MO and CIP was investigated. M2 was used to evaluate the adsorption–photocatalytic activity

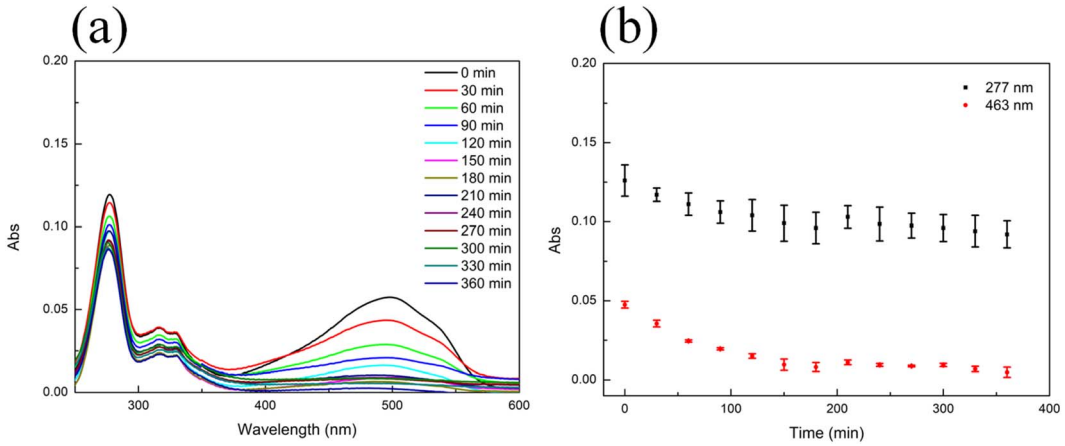

Fig. 8 (a) Temporal variation of the MO and CIP mixture's absorption spectrum and (b) kinetic curve of the mixture of MO and CIP solution in the presence of M2 under 180 min dark conditions and subsequent 180 min visible-light irradiation (initial concentration of MO and CIP: 1 mg L^{-1}).

of the Eu–TiO_2/PVDF membrane, as it showed relatively good adsorption and photocatalytic performance in former experiments. In this experiment, M2 was added into a mixture of the equiconcentrated MO and CIP solution (1 mg L^{-1}) and placed under stirring and dark conditions at first, subsequently, under visible-light irradiation. After 180 min of dark adsorption, the adsorption–desorption equilibrium reached and the mixture was placed under visible-light irradiation. It is worth noting that in the absence of the photocatalyst, the concentration of CIP or MO remains almost unchanged under visible-light irradiation (Fig. S8†). Fig. 8 shows the adsorption and photocatalytic degradation of the mixture of MO and CIP by M2. Fig. 8(b) was obtained by plotting the registered absorbance values at the maximum absorption wavelengths of CIP (277 nm) and MO (463 nm). It is important to underline that only MO absorbs light at 463 nm, while the absorbance at 277 nm stems from the contribution of both MO and CIP. The removal percentage of MO and CIP by M2 was 95% and 19%, respectively, after 360 min, namely after both the dark adsorption and photocatalytic experiments were performed.

In order to study the adsorption–photocatalytic kinetics of M2 towards MO, data were collected at 463 nm from 0 min to 360 min (Fig. 9(a)). In Fig. 9(a), the adsorption of MO by M2 accounted for a significant proportion. Therefore, the pseudo-first-order (eqn (2)) and pseudo-second-order (eqn (3)) models were selected to evaluate the adsorption–photocatalysis kinetics of M2 towards MO in this study. Fig. S11† and Table 7 show that the kinetic data are better fitted with a pseudo-second-order model than with a pseudo-first-order one: the correlation coefficient value of the pseudo-second-order model ($R^2 = 0.9582$) is higher than that of the pseudo-first-order one ($R^2 = 0.2837$). According to the pseudo-second-order model, the adsorption rate depends on the adsorption capacity not on the concentration of adsorbate and the rate-determining step in the adsorption process is the interaction of MO with the adsorption sites of M2.[27,29]

At 277 nm (maximum absorption value for CIP), both MO and CIP absorb light. Therefore, the absorbance of CIP at 277 nm was calculated by subtracting the absorbance of MO at 277 nm from the absorbance of the mixture of MO and CIP at

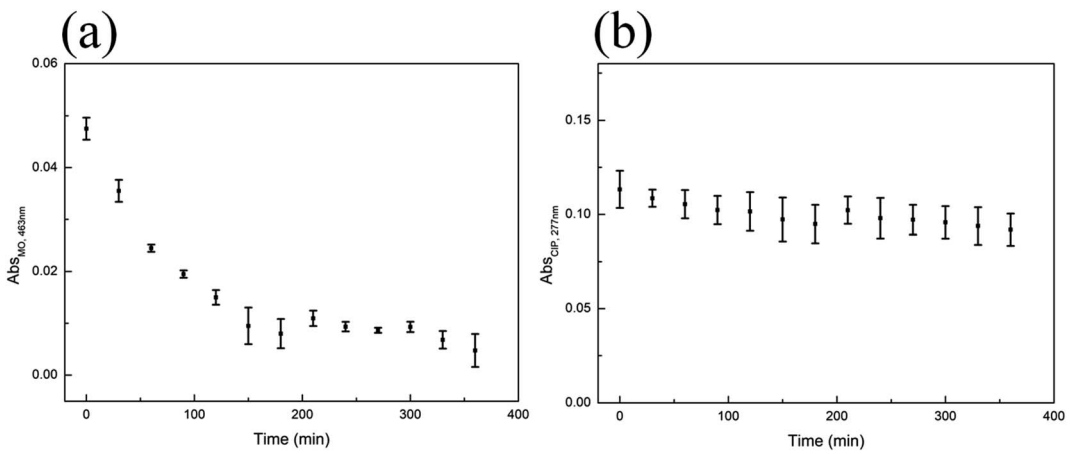

Fig. 9 Time-dependent variation of the absorbance of (a) MO at 463 nm and (b) CIP at 277 nm withdraw from a mixture of MO and CIP in the presence of M2 (initial concentration of MO and CIP: 1 mg L^{-1}).

Table 7 Model parameters of adsorption–photocatalysis kinetics for MO and CIP in the presence of M2

		Pseudo-first-order model			Pseudo-second-order model		
Pollutants	$q_{e,exp}$ (mg g^{-1})	q_e (mg g^{-1})	k_1 (min^{-1})	R^2	q_e (mg g^{-1})	k_2 (g (mg^{-1} min^{-1}))	R^2
MO	0.55	0.62	0.02253	0.2837	0.62	0.03538	0.9582
CIP	0.13	0.11	0.00592	0.6901	0.16	0.03545	0.4117

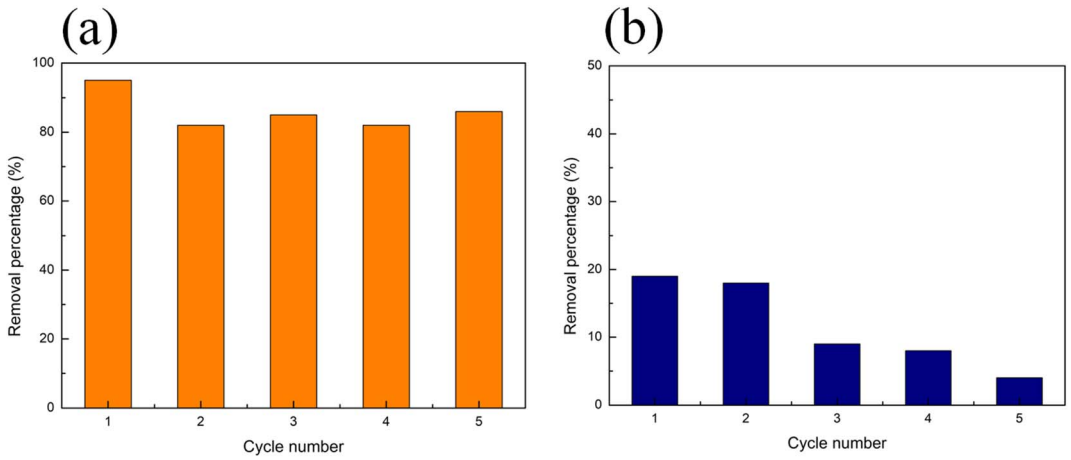

Fig. 10 Recycling experiments of M2 adsorbing–degrading a mixture of MO and CIP: removal percentage of (a) MO and (b) CIP.

the same wavelength (Fig. 9(b)). The pseudo-first-order (eqn (2)) and pseudo-second-order (eqn (3)) models were used to evaluate the adsorption–photocatalytic degradation kinetics of M2 towards CIP. Fig. S12† and Table 7 show that the kinetic data are better fitted with a pseudo-first-order model than with a pseudo-second-order one: the correlation coefficient value of the pseudo-first-order model ($R^2 = 0.6901$) results higher than that of the pseudo-second-order one ($R^2 = 0.4117$). According to the pseudo-first-order model, the rate of change of solute uptake with time is directly proportional to difference in saturation concentration and the amount of solid uptake with time, which is generally applicable over the initial stage of an adsorption process.[27] It is commonly observed that kinetics followed the pseudo-first-order model when adsorption occurs through diffusion through the interface.[27]

3.5 Reusability of the membranes

Based on the easy separation and recovery characteristics of the PVDF membrane, the Eu–TiO_2/PVDF membranes could be easily and quickly recycled and reused. In this work, we performed the recycling experiments to assess the adsorption–photocatalysis performance of the Eu–TiO_2/PVDF membrane (M2) over different adsorption–photocatalytic cycles. A mixture of MO and CIP was used as the model mixed pollutants for this experiment. M2 was utilised in the adsorption–photocatalytic degradation of a mixture of MO and CIP, recovered, washed with 0.1 M HCl and ultrapure water, and dried before being used for another adsorption–photocatalytic experiment with a fresh mixture of MO and CIP solution. This procedure was repeated for five times. The results for five adsorption–photocatalysis cycles are reported in Fig. 10. As shown in Fig. 10(a), the removal percentage of MO by M2 only slightly decreased with the number of reutilisations. After five cycles, the amount of removed MO decreased only 9%, namely from 95% to 86% of the initial MO amount. Fig. 10(b) shows that after five cycles, the amount of removed CIP decreased by 15%, namely from 19% to 4% of the initial CIP amount. The small decrease in the removal efficiency may be due to the loss of active sites caused by the adsorption on the surface of the catalyst of possibly unreacted MO/CIP and/or its degradation products.[8,43] These results indicated that the Eu–TiO_2/PVDF membrane possessed good stability and durability thus opening the path, after further studies, for a possible future industrial application.

4. Conclusions

In summary, Eu–TiO_2/PVDF membranes were prepared by the combination of the modified sol–gel method and the immersion phase inversion method. The obtained Eu–TiO_2/PVDF membranes were named M1, M2 and M3 with the increase of Eu–TiO_2 NPs content. Meanwhile, as a reference, the pure PVDF membrane (M0) was prepared by the immersion phase inversion method. The obtained membranes could not only adsorb MO, but also degrade CIP under visible-light irradiation. In details, the adsorption percentage of MO by M0, M1, M2 and M3 was 75%, 36%, 39% and 27% and the degradation efficiency of CIP by M1, M2 and M3 was 4%, 16% and 21%, respectively. In addition, the adsorption rate constant of MO in the presence of M0, M1, M2 and M3 was 0.01527, 0.01203, 0.01757 and

0.01181 min^{-1} and the degradation rate constant of CIP by M1, M2 and M3 was 3.2×10^{-6}, 6.9×10^{-4} and 8.8×10^{-4} min^{-1}. Moreover, the Eu–TiO_2/PVDF membrane (M2) showed adsorption–degradation activity towards a mixture of MO and CIP under visible-light irradiation. After 360 min of adsorption-degradation, the removal percentage of MO was 95% and the removal percentage of CIP was 19%, in the presence of M2. Finally, due to the use of PVDF membrane as a support, the Eu–TiO_2/PVDF membranes could be easily and quickly recycled and reused. After five cycles, the removal percentage of MO only decreased 9% and the removal percentage of CIP decreased 15%. It is foreseen that the Eu–TiO_2/PVDF membranes will find practical utilisation and application in water treatment.

Author contributions

Conceptualization: J. W.; data curation: J. W.; formal analysis: J. W., H. M. P., P. C. Z., N. Z.; funding acquisition: J. W.; investigation: J. W., H. M. P., P. C. Z., N. Z.; methodology: J. W., H. M. P., P. C. Z., N. Z.; project administration: J. W.; resources: J. W.; supervision: J. W.; validation: J. W.; visualization: J. W.; writing – original draft: J. W.; writing – review & editing: J. W.

Conflicts of interest

The authors declare no conflict of interest.

Acknowledgements

The authors gratefully acknowledge financial support from Natural Science Basic Research Program of Shaanxi, P. R. China (Program No. 2023-JC-QN-0570), Young Talent Fund of Xi'an Association for Science and Technology, P. R. China (Program No. 959202313040) and Shaanxi Province Scholarship Program for Science and Technology Activities of the Returned Overseas Chinese, P. R. China (Program No. 2022-026).

References

1 F. M. Drumond Chequer, G. A. R. de Oliveira, E. R. Anastacio Ferraz, J. Carvalho, M. V. Boldrin Zanoni and D. P. de Oliveir, Textile dyes: dyeing process and environmental impact, *Eco-Friendly Text. Dyeing Finish.*, 2013, **6**, 151–176.

2 C. R. Holkar, A. J. Jadhav, D. V. Pinjari, N. M. Mahamuni and A. B. Pandit, A critical review on textile wastewater treatments: possible approaches, *J. Environ. Manage.*, 2016, **182**, 351–366.

3 H. Salazar, P. M. Martins, B. Santos, M. M. Fernandes, A. Reizabal, V. Sebastián, G. Botelho, C. J. Tavares, J. L. Vilas-Vilela and S. Lanceros-Mendez, Photocatalytic and antimicrobial multifunctional nanocomposite membranes for emerging pollutants water treatment applications, *Chemosphere*, 2020, **250**, 126299.

4 J. Shen, Z. Li, Y. nan Wu, B. Zhang and F. Li, Dendrimer-based preparation of mesoporous alumina nanofibers by electrospinning and their application in dye adsorption, *Chem. Eng. J.*, 2015, **264**, 48–55.

5 M. S. Najafinejad, P. Mohammadi, M. Mehdi Afsahi and H. Sheibani, Green synthesis of the Fe_3O_4@polythiophen-Ag magnetic nanocatalyst using grapefruit peel extract: application of the catalyst for reduction of organic dyes in water, *J. Mol. Liq.*, 2018, **262**, 248–254.

6 R. Kumar, G. Kumar and A. Umar, ZnO nano-mushrooms for photocatalytic degradation of methyl orange, *Mater. Lett.*, 2013, **97**, 100–103.

7 L. Zhang, H. Li, Y. Liu, Z. Tian, B. Yang, Z. Sun and S. Yan, Adsorption-photocatalytic degradation of methyl orange over a facile one-step hydrothermally synthesized TiO_2/ZnO-NH_2-RGO nanocomposite, *RSC Adv.*, 2014, **4**, 48703–48711.

8 A. Kaur, W. A. Anderson, S. Tanvir and S. K. Kansal, Solar light active silver/iron oxide/zinc oxide heterostructure for photodegradation of ciprofloxacin, transformation products and antibacterial activity, *J. Colloid Interface Sci.*, 2019, **557**, 236–253.

9 W. Xu, G. Zhang, X. Li, S. Zou, P. Li, Z. Hu and J. Li, Occurrence and elimination of antibiotics at four sewage treatment plants in the Pearl River Delta (PRD), South China, *Water Res.*, 2007, **41**, 4526–4534.

10 J. Wang, L. Svoboda, Z. Němečková, M. Sgarzi, J. Henych, N. Licciardello and G. Cuniberti, Enhanced visible-light photodegradation of fluoroquinolone-based antibiotics and *E. coli* growth inhibition using Ag–TiO_2 nanoparticles, *RSC Adv.*, 2021, **11**, 13980–13991.

11 R. B. Rajput, S. N. Jamble and R. B. Kale, A review on TiO_2/SnO_2 heterostructures as a photocatalyst for the degradation of dyes and organic pollutants, *J. Environ. Manage.*, 2022, **307**, 114533.

12 S. K. Kansal, M. Singh and D. Sud, Studies on photodegradation of two commercial dyes in aqueous phase using different photocatalysts, *J. Hazard. Mater.*, 2007, **141**, 581–590.

13 B. Rani, S. Punniyakoti and N. K. Sahu, Polyol asserted hydrothermal synthesis of SnO_2 nanoparticles for the fast adsorption and photocatalytic degradation of methylene blue cationic dye, *New J. Chem.*, 2018, **42**, 943–954.

14 Y. Deng and R. Zhao, Advanced oxidation processes (AOPs) in wastewater treatment, *Curr. Pollut. Rep.*, 2015, **1**, 167–176.

15 J. Zhang, B. Tian, L. Wang, M. Xing and J. Lei, *Photocatalysis*, Springer, 2018.

16 J. C. Wang, H. H. Lou, Z. H. Xu, C. X. Cui, Z. J. Li, K. Jiang, Y. P. Zhang, L. B. Qu and W. Shi, Natural sunlight driven highly efficient photocatalysis for simultaneous degradation of rhodamine B and methyl orange using I/C codoped TiO_2 photocatalyst, *J. Hazard. Mater.*, 2018, **360**, 356–363.

17 J. Jing, J. Li, J. Feng, W. Li and W. W. Yu, Photodegradation of quinoline in water over magnetically separable Fe_3O_4/TiO_2 composite photocatalysts, *Chem. Eng. J.*, 2013, **219**, 355–360.

18 N. Hosseini Nasab, M. M. Jalili and S. Farrokhpay, Application of paraffin and silver coated titania nanoparticles in polyethylene nanocomposite food packaging films, *J. Appl. Polym. Sci.*, 2018, **135**, 1–7.

19 S. Wu, X. Li, Y. Tian, Y. Lin and Y. H. Hu, Excellent photocatalytic degradation of tetracycline over black anatase-TiO_2 under visible light, *Chem. Eng. J.*, 2021, **406**, 126747.

20 C. Jia, X. Zhang, K. Matras-Postolek, B. Huang and P. Yang, Z-Scheme reduced graphene oxide/TiO_2-Bronze/$W_{18}O_{49}$ ternary heterostructure towards efficient full solar-spectrum photocatalysis, *Carbon*, 2018, **139**, 415–426.

21 S. Karuppaiah, R. Annamalai, A. Muthuraj, S. Kesavan, R. Palani, S. Ponnusamy, E. R. Nagarajan and S. Meenakshisundaram, Efficient photocatalytic degradation of ciprofloxacin and bisphenol A under visible light using Gd_2WO_6 loaded ZnO/bentonite nanocomposite, *Appl. Surf. Sci.*, 2019, **481**, 1109–1119.

22 H. Nawaz, M. Umar, I. Nawaz, A. Ullah, M. Tauseef Khawar, M. Nikiel, H. Razzaq, M. Siddiq and X. Liu, Hybrid PVDF/PANI membrane for removal of dyes from textile wastewater, *Adv. Eng. Mater.*, 2022, **24**, 2100719.

23 D.-S. Zhen, M. Guo, X.-F. Li, H.-L. Mao, C.-A. Li, J.-L. Li and Y. Liu, Eu–TiO_2 nanocomposite with high photoelectrochemical activity for enhanced photocatalysis of rhodamine B, *J. Nanosci. Nanotechnol.*, 2019, **19**, 7758–7763.

24 J. Li, X. Liu, J. Lu, Y. Wang, G. Li and F. Zhao, Anti-bacterial properties of ultrafiltration membrane modified by graphene oxide with nano-silver particles, *J. Colloid Interface Sci.*, 2016, **484**, 107–115.

25 Y. Peng, Z. Yu, Y. Pan and G. Zeng, Antibacterial photocatalytic self-cleaning poly(vinylidene fluoride) membrane for dye wastewater treatment, *Polym. Adv. Technol.*, 2018, **29**, 254–262.

26 N. Li, Z. Li, L. Zhang, H. Shi, J. Li, J. Zhang, Z. Zhang and F. Dang, One-step fabrication of bifunctional self-assembled oligopeptides anchored magnetic carbon nanoparticles and their application in copper (II) ions removal from aqueous solutions, *J. Hazard. Mater.*, 2020, **382**, 121113.

27 T. R. Sahoo and B. Prelot, *Nanomaterials for the Detection and Removal of Wastewater Pollutants*, Elsevier, 2020.

28 H. Sun, Z. Ji, Y. He, L. Wang, J. Zhan, L. Chen and Y. Zhao, Preparation of PAMAM modified PVDF membrane and its adsorption performance for copper ions, *Environ. Res.*, 2022, **204**, 111943.

29 H. Yan, W. Zhang, X. Kan, L. Dong, Z. Jiang, H. Li, H. Yang and R. Cheng, Sorption of methylene blue by carboxymethyl cellulose and reuse process in a secondary sorption, *Colloids Surf., A*, 2011, **380**, 143–151.

30 B. Özkahraman, I. Acar and S. Emik, Removal of cationic dyes from aqueous solutions with poly(N-isopropylacrylamide-co-itaconic acid) hydrogels, *Polym. Bull.*, 2011, **66**, 551–570.

31 A. M. Atta, H. A. Al-Lohedan, Z. A. ALOthman, A. A. Abdel-Khalek and A. M. Tawfeek, Characterization of reactive amphiphilic montmorillonite nanogels and its application for removal of toxic cationic dye and heavy metals water pollutants, *J. Ind. Eng. Chem.*, 2015, **31**, 374–384.

32 P. Martins, S. Kappert, H. Nga Le, V. Sebastian, K. Kühn, M. Alves, L. Pereira, G. Cuniberti, M. Melle-Franco and S. Lanceros-Méndez, Enhanced photocatalytic activity of Au/TiO_2 nanoparticles against ciprofloxacin, *Catalysts*, 2020, **10**, 234.

33 L. Penboon, A. Khrueakham and S. Sairiam, TiO_2 coated on PVDF membrane for dye wastewater treatment by a photocatalytic membrane, *Water Sci. Technol.*, 2019, **79**, 958–966.

34 M. Yan, Y. Wu and X. Liu, Photocatalytic nanocomposite membranes for high-efficiency degradation of tetracycline under visible light: an imitated core-shell Au-TiO_2-based design, *J. Alloys Compd.*, 2021, **855**, 157548.

35 Y. Zhang, B. Yang, K. Li, D. Hou, C. Zhao and J. Wang, Electrospun porous poly(tetrafluoroethylene-co-hexafluoropropylene-co-vinylidene fluoride) membranes for membrane distillation, *RSC Adv.*, 2017, **7**, 56183–56193.

36 Y. Peng and P. Wu, A two dimensional infrared correlation spectroscopic study on the structure changes of PVDF during the melting process, *Polymer*, 2004, **45**, 5295–5299.

37 J. R. Mishra, S. K. Samal, S. Mohanty and S. K. Nayak, Polyvinylidene fluoride (PVDF)/Ag@TiO_2 nanocomposite membrane with enhanced fouling resistance and antibacterial performance, *Mater. Chem. Phys.*, 2021, **268**, 124723.

38 P. Pascariu, C. Cojocaru, P. Samoila, N. Olaru, A. Bele and A. Airinei, Novel electrospun membranes based on PVDF fibers embedding lanthanide doped ZnO for adsorption and photocatalytic degradation of dye organic pollutants, *Mater. Res. Bull.*, 2021, **141**, 111376.

39 L. A. Shah, T. Malik, M. Siddiq, A. Haleem, M. Sayed and A. Naeem, TiO_2 nanotubes doped poly(vinylidene fluoride) polymer membranes (PVDF/TNT) for efficient photocatalytic degradation of brilliant green dye, *J. Environ. Chem. Eng.*, 2019, **7**, 103291.

40 H. Zhao, D. Zhang, H. Sun, Y. Zhao and M. Xie, Adsorption and detection of heavy metals from aqueous water by PVDF/ATP-CDs composite membrane, *Colloids Surf., A*, 2022, **641**, 128573.

41 Y.-X. Wang, S. Ma, M.-N. Huang, H. Yang, Z.-L. Xu and Z. Xu, Ag NPs coated PVDF@TiO_2 nanofiber membrane prepared by epitaxial growth on TiO_2 inter-layer for 4-NP reduction application, *Sep. Purif. Technol.*, 2019, **227**, 115700.

42 J. Wang, M. Sgarzi, Z. Němečková, J. Henych, N. Licciardello and G. Cuniberti, Reusable and antibacterial polymer-based nanocomposites for the adsorption of dyes and the visible-light-driven photocatalytic degradation of antibiotics, *Global Challenges*, 2022, **6**, 2200076.

43 S. Hamzezadeh-Nakhjavani, O. Tavakoli, S. P. Akhlaghi, Z. Salehi, P. Esmailnejad-Ahranjani and A. Arpanaei, Efficient photocatalytic degradation of organic pollutants by magnetically recoverable nitrogen-doped TiO_2 nanocomposite photocatalysts under visible light irradiation, *Environ. Sci. Pollut. Res.*, 2015, **22**, 18859–18873.